Physics of the Earth and Planetary Interiors, 79 (1993) 335–347
Elsevier Science Publishers B.V., Amsterdam

Preliminary evidence for a lower mantle shear wave velocity discontinuity beneath the central Pacific

E.J. Garnero *[,a], D.V. Helmberger [a], S. Grand [b]

[a] *California Institute of Technology, Seismological Laboratory 252-21, Pasadena, CA 91125, USA*
[b] *University of Texas, Department of Geological Sciences, P.O. Box 7909, Austin, TX 78715, USA*

(Received 4 February 1993; revision accepted 18 March 1993)

ABSTRACT

In a dataset consisting of long-period waveforms (5–20 s) and differential travel times of S, ScS, and the arrival from the D″ layer, Scd, evidence is found for a laterally varying shear wave velocity (V_S) discontinuity at the base of the mantle. Two different localized D″ regions beneath the central Pacific have been investigated. Predictions from a model having a V_S discontinuity 180 km above the core–mantle boundary (CMB) agree well with observations for an eastern mid-Pacific CMB region. This thickness differs from V_S discontinuity thicknesses found in other regions, which average near 280 km. The data presented here from a western mid-Pacific CMB region are more complicated, and are difficult to fit with a one-dimensional (1-D) structure. Some of the data from the western region show evidence for a thicker D″ layer (approximately 280 km), though this finding is poorly constrained. Our data do not resolve the 'sharpness' of the V_S jump at the top of D″, i.e. the depth range over which the V_S increase occurs, and in fact may be modeled equally well by a lower mantle with the increase in V_S at the top of D″ occurring over a 100 km depth range. The Scd–S and ScS–S differential travel times were corrected for a published 3-D mantle model, to study upper and middle mantle heterogeneity effects on these times.

1. Introduction

Direct forward modeling as well as tomographic inversion results have indicated that the velocity structure of the lowermost 100–300 km of the mantle (the D″ region) beneath the central Pacific is very anomalous in comparison to global Earth averages (see, for example, Dziewonski, 1984; Hager et al., 1985; Dziewonski and Woodhouse, 1987; Giardini et al., 1987; Tanimoto, 1990; Woodward and Masters, 1991; Li et al., 1991; Su et al., 1992; Garnero and Helmberger, 1993). In these studies, the central Pacific D″ region is characterized by having slower than average seismic velocities with bordering regions that are faster than average. Such patterns have important implications for the temperature distribution, and therefore, convection patterns in the lower mantle. Constraining the details of the D″ structure in these regions, such as the possible existence of a shear wave V_S discontinuity, will have relevance to any mid-Pacific convection model (e.g. Sleep, 1988; Olsen and Kincaid, 1991).

We utilize waveforms of direct S and core-reflected ScS seismic phases, along with observations of an arrival intermediate in time to S and ScS, termed Scd by Lay and Helmberger (1983). The raypath of Scd is very similar to ScS except that it bottoms above the core–mantle boundary (CMB) within the D″ layer. The timing and amplitude of the Scd arrival have been used in detailed modeling studies of V_S structure for many different D″ regions (e.g. Lay and Helmberger, 1983; Young and Lay, 1987, 1990; Weber and Davis, 1990; Gaherty and Lay, 1992). Figure 1 shows regions where D″ discontinuities in V_S have been proposed in past studies, along with the proposed V_S structures. Also presented in Fig. 1 are the two localized central Pacific regions investigated in this study. The details of the mod-

* Corresponding author.

els differ, such as depth of discontinuity and velocity gradients, indicating the degree of lateral heterogeneity encountered in the lower mantle.

The primary purpose of this paper is to present preliminary evidence for a V_S discontinuity in D″ beneath the central Pacific. The data for the more easterly patch in Fig. 1 are interpreted to suggest an average V_S structure having a discontinuity around 180 km above the CMB. This D″ layer is much thinner than structures presented in other areas (e.g. 250–320 km thick, averaging around 280 km thick; see Fig. 1). The data for the more westerly CMB region behave less uniformly, but give tentative evidence for a D″ layer having a more conventional thickness, possible around 280 km. These observations are discussed in more detail in following sections.

In a previous study, Garnero et al. (1988) proposed a lower mantle model beneath the Pacific whereby a V_S discontinuity in regions bordering the Pacific "fades away" to no discontinuity in the mid-Pacific (model SGHE, Fig. 1). This was based on anomalously large S–SKS times which were interpreted as being due to anomalously slow S waves, along with a lack of waveform evidence at 92° for a discontinuity arrival that has been observed in other D″ discontinuity studies (e.g. Lay and Helmberger, 1983; Young and Lay, 1987; Gaherty and Lay, 1992). For these reasons, Garnero et al. (1988) favored a central Pacific D″ region not having a V_S discontinuity. The large S–SKS times of Garnero et al. (1988), however, can be explained even if a D″ discontinuity exists. The large travel-time anomalies may be due to lateral changes in mantle velocity such as those derived from tomographic studies. Also, the absence of a double arrival at 92° can be produced by a model with a thin D″ discontinuity, which in turn delays the triplication normally seen at 92° to a larger distance, such as 98° for a D″ discontinuity 180 km above the CMB. (Such affects were explored by Lay and Young (1991) for the SYLO region beneath Alaska, Fig. 1.) This 98° double arrival can be further affected, and reduced to a single arrival, by smearing the step increase in V_S at the top of the D″ fast layer over a 50–100 km depth range. Observations of anomalously slow mid-Pacific S times and the

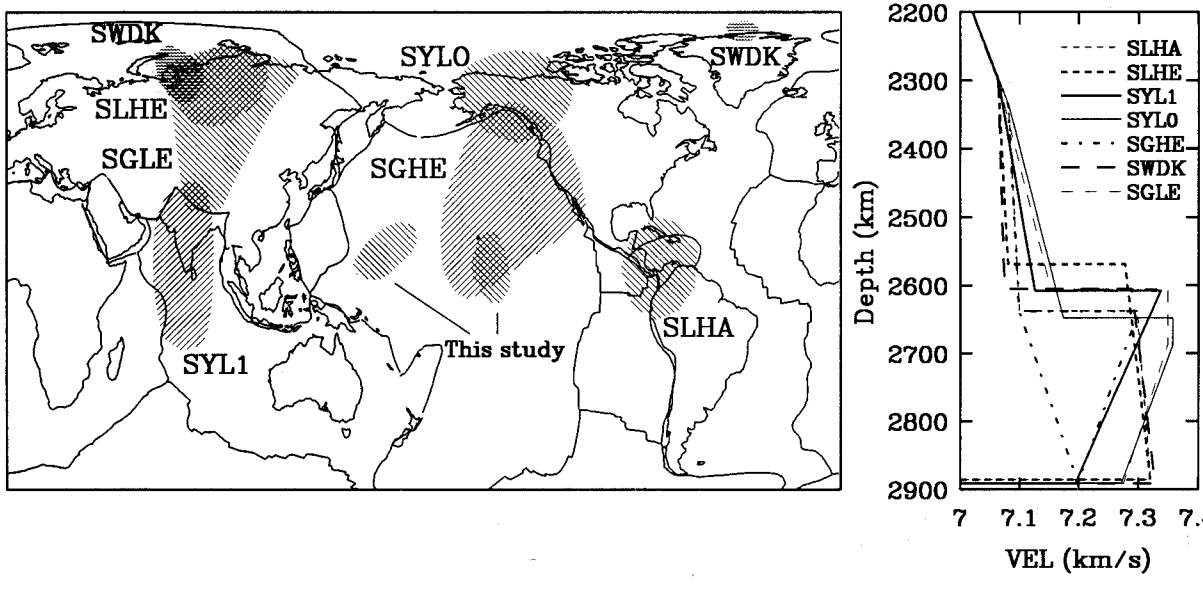

Fig. 1. Map of the world showing regions of D″ where V_S discontinuities have been proposed. The two small regions in the central Pacific are investigated here. The hatched regions are labeled with the name of the model derived for that region. The V_S profiles for these models are plotted on the right.

non-existence of the Scd arrival at 92° can thus be reconciled with a model containing a D″ discontinuity.

2. One-dimensional (1-D) synthetics

The approach taken here is to compare synthetic seismograms to observations in a forward modeling process. Particular attention is given to SH motions, since reflection coefficients for ScS and Scd are the largest for this type of motion, making it ideal to investigate deep mantle discontinuities. Some SV records were analyzed, though our data selection has been biased to gather SH-rich events for our source–receiver geometries in an effort to facilitate investigating V_S discontinuity structure in D″.

Figure 2 shows the SH predictions of four models for a source depth of 500 km: models PREM (Dziewonski and Anderson, 1981), SYL1 (Young and Lay, 1987), and two new models having a thinner D″ layer, SGHP and SGRD. PREM was chosen to represent structures not having a V_S discontinuity in D″. SYL1 is utilized to represent a D″ having a commonly found thickness of around 280 km. Model SGHP is similar to SYL1 with the notable exception being the reduced thickness of the D″ layer (180 km). The fourth model SGRD is similar to SGHP except the increase in V_S at the top of D″ in SGRD is distributed over a 100 km gradient transition zone. The generalized ray method was used (see Helmberger, 1983) to produce the synthetics, which were then convolved with the long-period (LP) World Wide Seismographic Station Network (WWSSN) instrument response. Most of the data analyzed in this study are LP WWSSN, so particular attention will be focused on the LP synthetics. As originally pointed out by

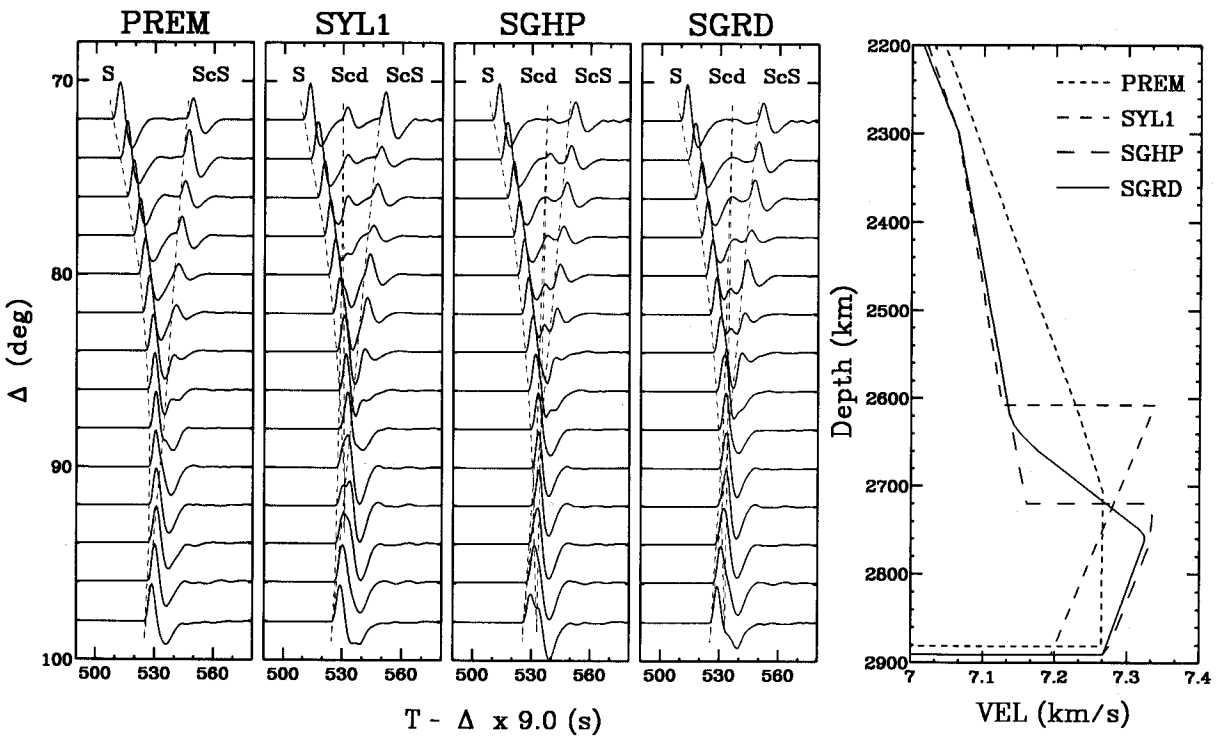

Fig. 2. SH component long-period WWSSN generalized ray synthetics for PREM (Dziewonski and Anderson, 1981), SYL1 (Young and Lay, 1987) and SGHP (this study). The presence of a thinner D″ discontinuity delays the arrival time of Scd as seen in the SGHP synthetics compared with SYL1.

Lay and Helmberger (1983) (and subsequent studies as well), a 2.7% V_S increase approximately 270 km above the CMB produces an arrival between S and ScS in the 70–84° distance range, as well as an observable double arrival near 92°. These effects can be seen in the SYL1 predictions of Fig. 2. The SGHP predictions differ from the SYL1 predictions most notably in the timing of the Scd phase. Owing to a thinner D″ fast layer, SGHP produces an Scd arrival later in time than that of SYL1 in the 70–84° distance range, and moves the double arrival effect seen at 92° in the SYL1 synthetics, to around 98°. By smearing the V_S increase at the top of D″ into a gradient 100 km thick, as in model SGRD, the amplitude of the Scd arrival is slightly reduced, especially at the tips of the Scd triplication branches, as seen at 74 and 98° (Fig. 2). However, the S, ScS, and Scd SH waveforms and travel times for model SGRD are almost identical to that of model SGHP in the distance range 76–96°. In the following section, synthetics calculated for the appropriate distances and source depths are compared with the observations for the three source–receiver geometries.

3. Data-set

Data samples are presented here from three source–receiver geometries having raypaths that traverse the central Pacific lower mantle: (1) records from Fiji–Tonga events recorded at west coast North American stations; (2) Java Sea, Banda Sea, and Philippine Islands events recorded at the central Pacific station KIP (Kipapa, Hawaii); (3) Sea of Okhotsk and Sea of Japan events recorded at the southwest Pacific station AFI (Afiamalu, Samoa). The event and station information for data presented in this section is given in Table 1. All events used are deep focus except for two intermediate depth events. The data used were recorded by LP WWSSN and LP Benioff 1-90 seismometers of the Caltech Network, which are both ideal in frequency response for detecting the Scd seismic

TABLE 1

Event and station information of data used in this study

Event code	Station	Δ (deg)	Az (deg)	Instrument code [a]	Date (mmddyy)	Depth (km)	Latitude	Longitude	M_b	Event region
F1	LON	78.4	34.2	LPWW	061584	247	−15.82	−174.83	6.1	Fiji–Tonga
F2	COR	78.8	36.1	LPWW	042584	415	−17.31	−177.23	5.7	Fiji–Tonga
F3	BKS	78.8	42.3	LPWW	100781	620	−20.75	−178.63	6.1	Fiji–Tonga
F4	BKS	79.2	42.4	LPWW	082885	625	−21.01	−178.98	6.2	Fiji–Tonga
F5	BKS	79.9	42.6	LPWW	062870	587	−21.66	−179.42	5.8	Fiji–Tonga
F6	PAS	79.9	47.5	B190	100967	605	−21.10	−179.18	6.2	Fiji–Tonga
F7	RVR	80.4	48.0	B190	100967	605	−21.10	−179.18	6.2	Fiji–Tonga
F8	LON	80.9	35.0	LPWW	042584	415	−17.31	−177.23	5.7	Fiji–Tonga
F9	BAR	81.3	48.2	B190	081267	144	−24.79	−177.38	6.0	Fiji–Tonga
F10	DAL	93.1 [b]	56.7	LPWW	085263	557	−17.58	−178.73	6.1	Fiji–Tonga
F11	DAL	95.9 [b]	57.2	LPWW	022275	333	−23.98	−178.88	6.1	Fiji–Tonga
F12	DAL	96.1 [b]	57.2	LPWW	012469	587	−21.87	−179.54	5.9	Fiji–Tonga
F13	DAL	97.4 [b]	57.6	LPWW	032374	504	−23.93	179.88	6.0	Fiji–Tonga
K1	KIP	75.8	70.1	LPWW	092073	560	9.05	123.79	6.0	Philippine Islands
K2	KIP	76.2	69.9	LPWW	030584	649	8.15	123.76	6.5	Philippine Islands
K3	KIP	79.7	66.8	LPWW	062282	450	−7.34	126.04	6.8	Banda Sea
A1	AFI	73.1	142.5	LPWW	090570	580	52.23	151.43	6.2	Sea of Okhotsk
A2	AFI	72.9	142.6	LPWW	122175	554	51.94	151.58	6.4	Sea of Okhotsk
A3	AFI	75.5	121.3	LPWW	062975	560	38.76	129.99	6.5	Sea of Japan

[a] LPWW = long-period WWSSN seismometer; B190 = Benioff 1-90 seismometer.

[b] Adjusted to 500 km source depth.

phase. The traces were optically scanned from paper records, digitized, then rotated to the source–receiver azimuth to obtain the natural radial and longitudinal components.

The different source–receiver geometries and raypaths of data are presented in Fig. 3. The great circle raypaths are indicated by the dotted lines, with the mid-points of the raypaths indicated by a shaded ellipse. The dimensions of the ellipse minor and major axes on the Earth's surface are approximately 200 and 1000 km, respectively, and roughly 100 by 500 km at the depth of the CMB. As the figure indicates, there are two primary CMB regions of study: a western central Pacific region sampled by the KIP and AFI data, and an eastern central Pacific region sampled by the North American data. In gathering AFI and KIP analog LP WWSSN records for studying the western CMB region, a limiting factor is the low gain of the instruments at both stations. This in turn requires gathering events as large as $M_b = 6.8$ to insure proper signal-to-noise ratio for these two stations. With records from the larger deep focus events often being more complex in waveshape, the data presented for this region are sparse. In investigating the eastern central Pacific D″ region of Fig. 3, the limiting factor in the data selection process is that data at less than 78° in distance are unavailable. Distance profiles of data are thus limited for this source–receiver azimuth to distances greater than this minimum distance. Because of these limitations, waveform modeling results for this path geometry are less unique than those having an epicentral distance range available that also spans the smaller distances, such as path geometries of the other study areas in Fig. 1. Nevertheless, first-order model features may be addressed for this geometry.

Data are first presented for the more abundantly sampled eastern central Pacific D″ region.

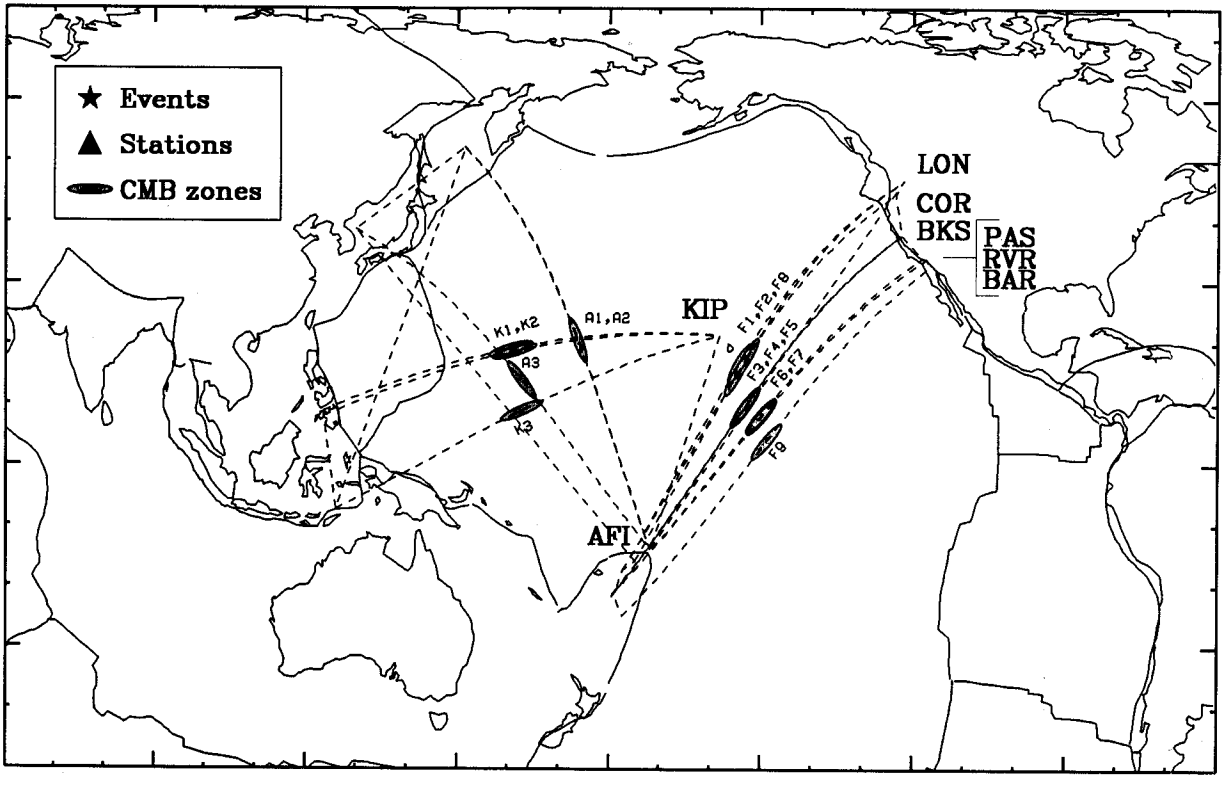

Fig. 3. Events, stations and great circle ray paths (dotted lines) are plotted along with ellipses depicting the CMB mid-point regions of the paths. The ellipses are accompanied with a letter–number code that corresponds to event and station information in Table 1.

Figure 4 displays the North American SH observations of Fiji–Tonga events (top bold traces). The traces are labeled with a letter–number code that corresponds to Table 1 and Fig. 3 (F1 through F9), and the epicentral distance and event source depth are printed above each panel of traces. Plotted along with the data are generalized ray synthetics using models SGHP, SYL1, and PREM. Synthetics from model SGRD are not included in the figure because the SGHP and SGRD synthetics fit the observations equally well. The data and synthetics have been lined up on the first arrival S-wave, and maximum amplitudes have been normalized to unity. The data show evidence for an arrival between S and ScS (denoted by a black dot), which is not predicted by the smooth D″ structure in PREM. Black dots also denote the Scd arrivals in the SGHP and SYL1 synthetics. The observed differential times of Scd–S are better modeled by the thinner D″ discontinuity in SGHP than that in SYL1 for this path geometry. However, timing and amplitude anomalies are present in Scd, as well as ScS, indicating the shortcomings of trying to fit the observations with a 1-D model for a region known to be anomalous. For example, for the record F4, the amplitude ratio of Scd/S is larger than the synthetic for model SGHP, which best predicts the differential time of Scd–S. However, for record F5, the Scd/S ratio is larger in the SGHP synthetics. Such amplitude variations may be an indication of the scale length over which lower mantle lateral variations occur. Also, records F8 and F9 display an anomalously large differential

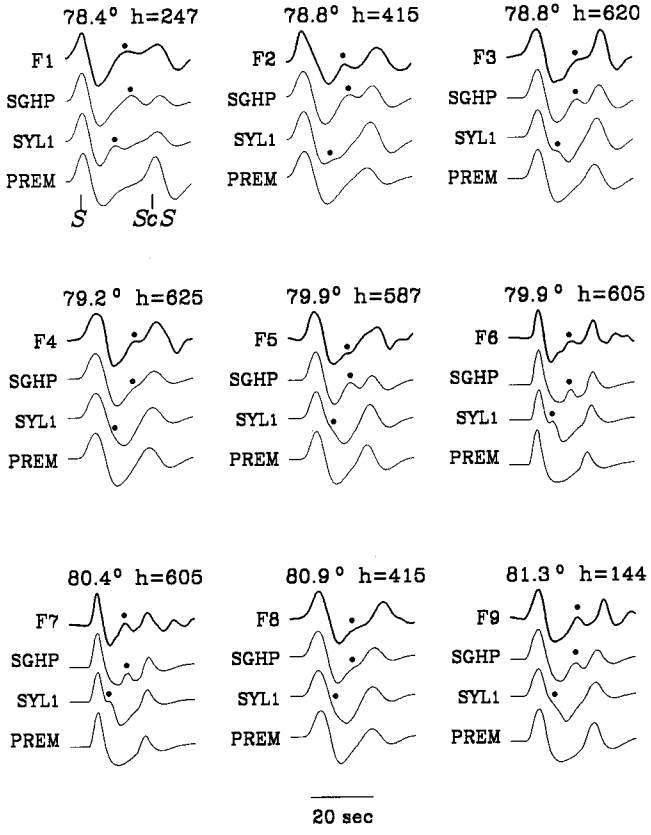

Fig. 4. SH data (top bold traces) and synthetics (models SGHP, SYL1 and PREM) comparison for the Fiji–Tonga data recorded at North American stations. The data are labeled to correspond to information in Table 1. The epicentral distance and source depth are printed above each panel. Black dots indicate the Scd arrival.

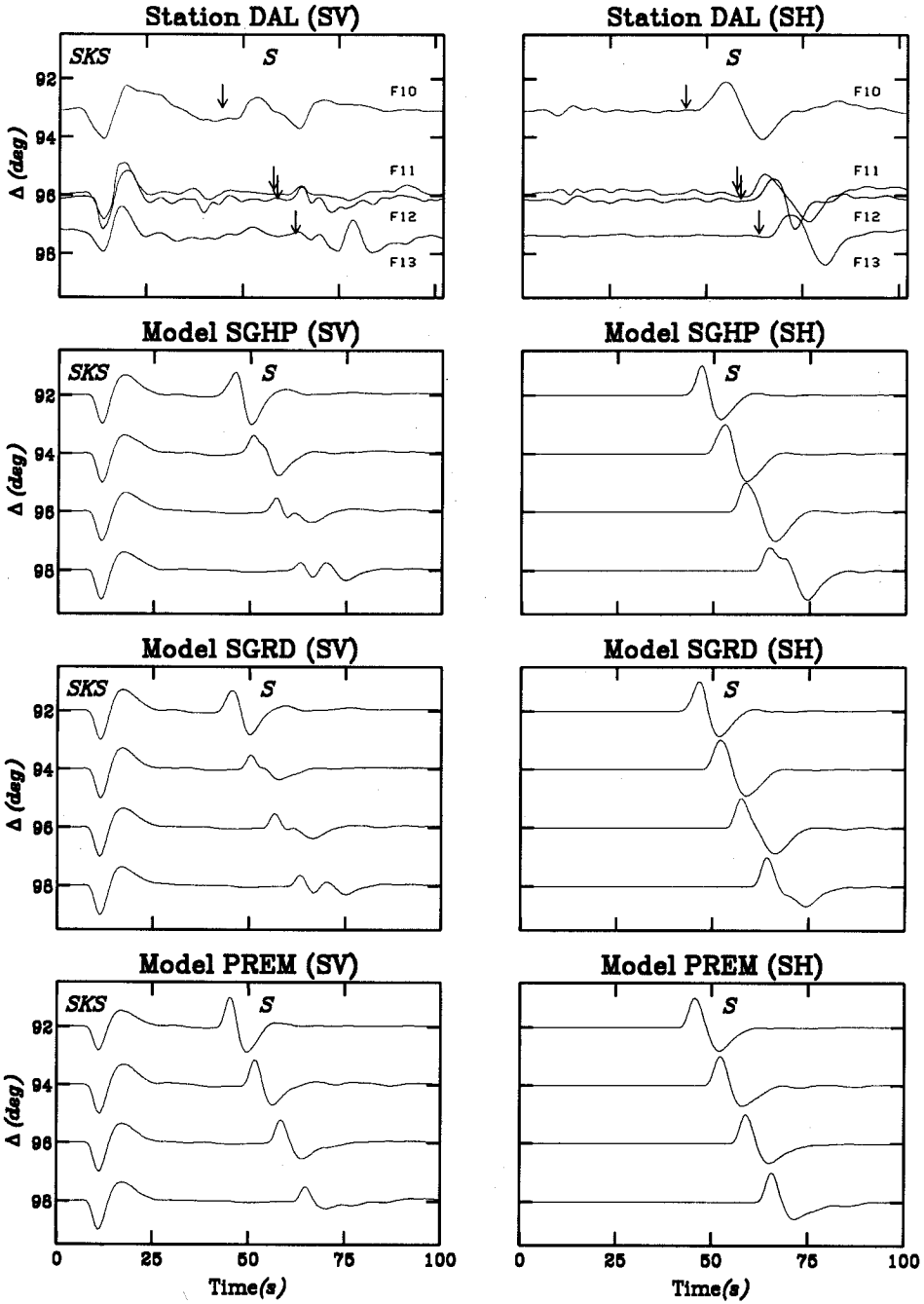

Fig. 5. Radial and transverse recordings from Fiji–Tonga events recorded at station DAL (top row), and synthetics for the models SGHP, SGRD and PREM (bottom three rows) are displayed in the 92–98° distance range. Arrows indicate the S–SKS time correction of model SH12_WM13 by Su et al. (1992); the arrow points to the corrected S time relative to SKS, which agrees better with synthetics.

travel time of ScS–S in comparison with the synthetics. This may be owing to an anomalously slow central Pacific lower mantle (as in Garnero and Helmberger, 1993) and will be further discussed in the travel-times section of this paper. Nevertheless, the relative timing of S, Scd, and ScS in the observations presented in Fig. 4 are fit in an average sense by model SGHP. The details of model SGHP, however, are not well constrained. The gradients above and below the D″ discontinuity can affect the relative amplitude ratios; as Fig. 2 indicates, we are unable to resolve such gradients with the LP data in the intermediate distance range.

We have investigated Fiji–Tonga data at larger distances to look for the double arrival seen at 98° in the SGHP SH synthetics of Fig. 2. The SH data we reviewed do not show conclusive evidence for a double arrival. However, there does appear to be a broadening of the SH waveform relative to SKS. Figure 5 shows a sample of the data at the North American station DAL (Dallas, Texas). Radial and tangential profiles are shown for four events recorded at DAL (top row), and for synthetics from models SGHP, SGRD, and PREM (the following three rows). The data have been adjusted to correspond to a 500 km source depth to compare with synthetics. All maximum amplitudes have been normalized to unity, and traces are lined up on the SKS arrival. The radial traces have been included because the discontinuity models predict a double arrival in SV at distances greater than 94°. The period of the synthetics has been adjusted to fit the SKS obser-

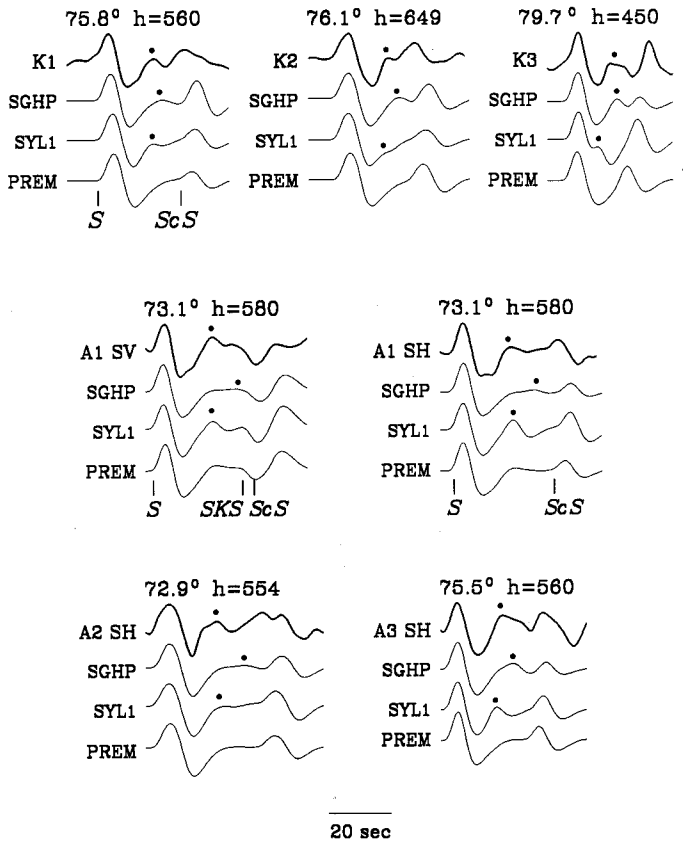

Fig. 6. SH data (top bold traces) and synthetics (models SGHP, SYL1 and PREM) comparison for the southwest Pacific events recorded at station KIP, and northwest Pacific events recorded at stations AFI. The data are labeled to correspond to information in Table 1.

vations roughly, except for F10 which appears anomalous. Note that simple models such as PREM predict SH waveforms nearly identical to the SKS observations except that they are inverted. The SH observations clearly display some broadening relative to SKS. If this were due to diffraction alone, the PREM SH synthetics should predict this broadening effect. For a 500 km source depth and the distance range presented in Fig. 5, the contribution to S-wave broadening in the PREM SH synthetics from diffraction is predicted to be negligible or non-existent. The SH record F13 is best fit by SGHP. The DAL SV data show complexities in the direct S-wave that are not seen in the PREM synthetics. The SGHP and SGRD SV predictions are very similar, and perhaps fit the data better than PREM. However, the complicated SV observations may indicate the difficulty encountered when attempting to model these data with 1-D synthetics in a region where the lower mantle is thought to be very anomalous. There are other difficulties in the interpretation of S-wave broadening being due to the presence of an Scd phase. The broadening of S relative to SKS is common owing to greater attenuation effects on the longer path of S in the mantle. Also, the spectrum of waves diffracted along the CMB is modified differently depending on the velocity gradient in D″ (see, for example, Doornbos and Mondt, 1979).

The S–SKS times for the mid-Pacific lower mantle region are anomalously large (Garnero et al., 1988; Garnero and Helmberger, 1993), as can be seen in the DAL data when compared with the synthetics in Fig. 5. Correcting the DAL S–SKS time observations for the 3-D mantle model of Su et al. (1992) produces S–SKS times similar to the synthetic predictions. The 3-D model S–SKS time corrections are indicated in the DAL data panels of Fig. 5 by arrows denoting the adjusted S times with respect to SKS.

Data from the two source–receiver geometries used to study the western CMB region are presented in Fig. 6. The labeling and plotting conventions are the same as in Fig. 4. The two SH KIP records K1 and K2 are at ideal distances for studying the Scd arrival. For these two records, the timing of Scd is closest to the predictions of SYL1. The timing of Scd for record K3 appears closer to that of SGHP, but is ambiguous owing to the complex Scd waveshape, which may be related to the size of the source ($M_b = 6.8$). Since record K3 has a D″ bounce point for Scd that is around 800 km to the south of records K1 and K2, lateral variations in D″ thickness may be contributing to the anomalous observation. Observations at station AFI from northwest Pacific events are presented in Fig. 6 as A1 SV, A1 SH, A2, and A3. For A1 SV and SH, model SYL1 produces the best fit of the three models, with the Scd–S time for that model most closely matching the observations. The SH records A2 and A3 are more complicated in waveshape but still show strong evidence for an Scd arrival. The A2 Scd–S time is closer to that of SYL1, though A3 has a time intermediate to the predictions of SYL1 and SGHP. The recordings A1, A2, and A3 are from relatively large events ($M_b = 6.2$, 6.4, and 6.5, respectively), which may be related to the waveform complexities. More data are needed to improve modeling of the western CMB region. The data presented in Fig. 6 may ultimately be better modeled by a D″ layer with a thickness closer to that of SYL1 (280 km). However, the travel-time and waveform variations in our small number of samples for this western region precludes any confident determination of D″ layer thickness.

4. Travel times and 3-D structure

The data in Fig. 4 suggest that the eastern CMB region in this study (see Fig. 1) may be better modeled by a D″ layer about 180 km thick. The data in Fig. 6, however, are less uniform indicating that the western CMB region may be too complicated to model with a 1-D structure. In this section we present raw differential travel times with respect to the 1-D structures SYL1 and SGHP, then correct the travel times for the 3-D mantle structure of Su et al. (1992).

The travel times of S, Scd, and ScS were measured by a procedure similar to Grand and Helmberger (1985): (1) line up the first arrival S-wave of the observation and the appropriate

synthetic seismogram; (2) pick the peak times of the Scd and ScS phases for each of the observations and synthetics; (3) take the differences $T_{OBS}(Scd) - T_{SYNTH}(Scd)$ and $T_{OBS}(ScS) - T_{SYNTH}(ScS)$. Figure 7 presents the travel times of the data with respect to SYL1 and SGHP predictions (solid and dotted lines, respectively). All S times have been lined up with that of SYL1 to study the differential times. The observed times have all been adjusted to correspond to a source depth of 500 km. Different symbols are used corresponding to the different paths of Fig. 3: crosses for the Fiji–Tonga data recorded in North America; diamonds for the southwest Pacific events recorded at KIP; circles for the northwest Pacific events recorded at AFI. No corrections for 3-D structure have been included in this figure. As seen in Fig. 4, the Scd–S times of the Fiji–Tonga data are more compatible with SGHP. The Scd–S times of the KIP and AFI data are better predicted by SYL1. The ScS–S times of the observations, however, are anomalous with respect to the predictions and will be explored below.

The 3-D mantle model of Su et al. (1992)

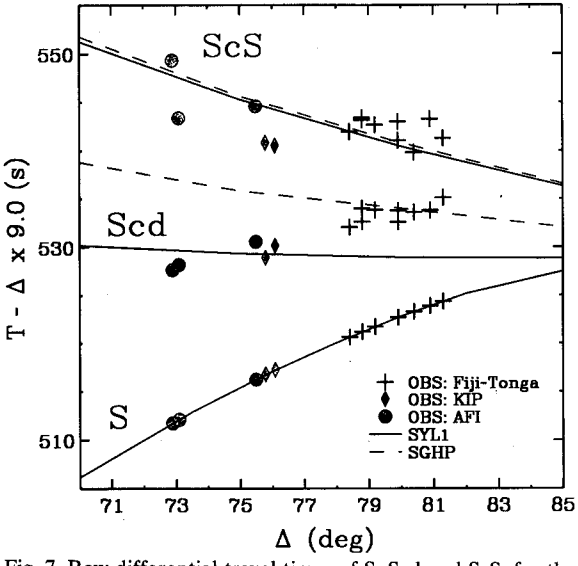

Fig. 7. Raw differential travel times of S, Scd and ScS, for the data of Figs. 4 and 6, compared with predictions of SYL1 (solid lines) and SGHP (dotted lines). All S times have been aligned with those of SYL1.

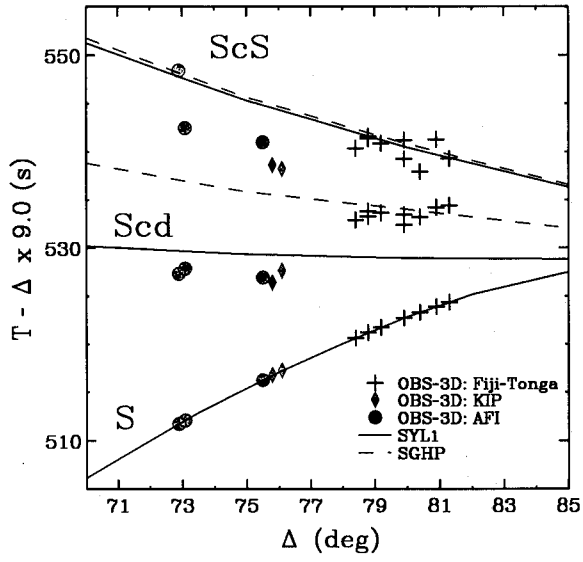

Fig. 8. Differential travel times of S, Scd and ScS, for the data of Figs. 4 and 6, corrected for the 3-D mantle model of Su et al. (1992), compared with predictions of SYL1 (solid lines) and SGHP (dotted lines). All S times have been aligned with those of SYL1.

(SH12_WM13) was used to make differential travel-time predictions for Scd–S and ScS–S. SH12_WM13 was shown to account for the general long-wavelength behavior of anomalous S–SKS times in the mid-Pacific (Garnero and Helmberger, 1993), and hence is utilized here in an effort to subtract out 3-D mantle contributions to the Scd–S and ScS–S differential travel times. The model was parameterized into 116 spherical shells vertically (25 km thick each) and laterally by blocks of dimension $2.5° \times 2.5°$. This grid is then used to calculate travel-time anomalies for laterally homogeneous raypaths of S, Scd, and ScS. The resulting residuals were subtracted from the observations and are presented in Fig. 8.

For the Fiji–Tonga data, model SH12_WM13 reduces the scatter in the Scd–S times and shifts the ScS–S times so that they agree better with predictions. Large travel-time anomalies are still present after correction, which may indicate the presence of anomalies of wavelength smaller than those presently resolvable by tomographic models. For the AFI and KIP data, after SH12_WM13 corrections, the Scd–S times reduce to about 2.5 s less than that of SYL1, and the ScS–S times on

average are about 5.5 s less than SYL1 predictions. With such few data, these times will not be used to infer a structure. However, it is interesting to note that a D″ layer thicker than that of SYL1 will reduce both the Scd–S and ScS–S times. A change in the V_S gradient in D″ of SYL1 from its present negative value to zero will also cause a reduction in the ScS–S time by 2.6 s (at 80°). Therefore a faster and thicker D″ layer would do better at predicting these times. Alternatively, an upper mantle that is slower than SH12_WM13 will slow down S-waves relative to Scd and ScS, reducing Scd–S and ScS–S times, thus better predicting the observations. More data (analog and digital) for this region are necessary to help identify the travel-time trends. Absolute timing information can then be used to help resolve the anomalies.

5. Discussion

As summarized by Gaherty and Lay (1992), many seismic structure scenarios can produce arrivals between S and ScS in the distance range 75–82° which may be misinterpreted as Scd arrivals. One case is that of slab diffraction discussed by Cormier (1989). Slab diffraction produces a double arrival from multipathing effects. Paths to the North American stations from the Tonga trench spend very little time in the slab, since the slab dips towards the west, striking around N15°E, and raypaths depart easterly from the underside of the slab. The azimuth range (relative to slab strike) of stations used here is such that slab effects are predicted to be absent (or small) (Cormier, 1989). The same path geometry in relationship to the slab orientation should be true for the three northwest Pacific events recorded at station AFI, and recordings K1 and K2 recorded at KIP. Record K3, however, has a path geometry that may be affected by slab multipathing. It has a complex Scd waveform and therefore was not used in the travel-time analysis.

Another scenario is that proposed by Haddon and Buchbinder (1987), whereby S-waves are scattered by 3-D heterogeneities at the base of the mantle, producing another arrival. Such phenomena may exist for this central-Pacific D″ region. However, for our dataset, the arrival we interpret as Scd has moveout as expected for a triplication arrival, and is observed with some regularity at the west coast United States stations for the Fiji–Tonga events. Deep mantle heterogeneities may be responsible for the variabilities seen in the observations from station to station, as well as small-scale scatter for this study area (see Garnero and Helmberger, 1993). It is our interpretation that the seismic arrival observed between S and ScS in the 78–82° distance range is most easily explained by a discontinuity in V_S at the top of D″.

The region slightly to the west, northwest, and southwest of our western CMB region was investigated by Revenaugh and Jordan (1991), where they reported that only five of their 18 source–receiver geometries support a lower mantle V_S discontinuity from a reverberation analysis of close-distance, SH-polarized multiple ScS waves. Their finding can be compatible with a ubiquitous D″ discontinuity in the region if the vertical dimension over which the jump in V_S occurs at the top of D″ is smeared over 50–100 km. This dimension would obscure evidence of the Scd arrival at near vertical incidence, as well as at the smallest (70–75°) and largest (near 92° for a 280 km thick D″) distances where Scd is routinely identified in studies that involve wide angles of incidence to D″. This feature, however, will still produce an Scd arrival in the 75–80° distance range. Revenaugh and Jordan (1991) reported that the five paths showing evidence for a D″ discontinuity are accompanied by different D″ thicknesses, from 270 to 340 km ($\pm$25 km). Perhaps the complexities in the data of Fig. 6 are related to such a variable D″ layer. Lateral variation in D″ thickness relates to many other disciplines of deep Earth study, and directly relates to studies concerned with D″ as a 'reservoir' for old slabs, or reaction products from chemical reactions between the liquid outer core and the crystalline silicates of the lowermost mantle (e.g. Knittle and Jeanloz, 1991). The preliminary finding here is that D″ thickness may vary by as much as 150 km between two distinctly different regions (e.g. see models SLHE and SGHP). This is larger than

previously noted for regions where D″ discontinuities have been proposed.

Several different factors may contribute to uncertainties in the travel-time measurements. For example, a 50 km error in source depth will result in an approximately 0.5 s error in both Scd–S and ScS–S. Travel-time picking errors may be as large as ±1.5 s for complicated records. Compounding these errors to obtain a ±2 s error bound on the differential travel-time measurements does not change our basic conclusions about lateral variations in D″ thickness beneath the mid-Pacific. CMB topography will affect the ScS times, which are not used here to infer D″ thickness.

6. Conclusions

In this study, we present preliminary evidence for a D″ discontinuity in V_S for two different regions beneath the central Pacific. The 3-D mantle model of Su et al. (1992) was used to correct the Scd–S and ScS–S differential travel times in an effort to isolate contributions to these times from D″ structure. Data traversing the CMB region to the east are best modeled by a D″ discontinuity around 180 km above the CMB. The data from the western region have significant scatter, precluding a confident estimate of a D″ layer thickness, though ultimately they may be better modeled by a D″ layer having a thickness closer to that of SYL1. The gradients above and below the D″ discontinuity, as well as the depth range over which the V_S increase at the top of the D″ discontinuity occurs, are not resolvable with the LP data. Future studies involving larger datasets, along with broadband data, may help to resolve such issues, as well as the lateral extent of such structures.

Acknowledgments

The authors thank Wei-jei Su for supplying the Su et al. (1992) model, along with necessary conversion subroutines. The comments of an anonymous reviewer improved the manuscript. Contribution 5260 of the Division of Geological and Planetary Sciences, California Institute of Technology, Pasadena, CA, USA.

References

Cormier, V.F., 1989. Slab diffraction of S waves. J. Geophys. Res., 94: 3006–3024.

Doornbos, D.J. and Mondt, J.C., 1979. Attenuation of P and S waves diffracted around the core. Geophys. J. R. Astron. Soc., 57: 353–379.

Dziewonski, A.M., 1984. Mapping the lower mantle: determination of lateral heterogeneity in P velocity up to degree and order 6. J. Geophys. Res., 89: 5929–5952.

Dziewonski, A.M. and Anderson, D.L., 1981. Preliminary reference Earth model (PREM). Phys. Earth Planet. Inter., 25: 297–356.

Dziewonski, A.M. and Woodhouse, J.H., 1987. Global images of the Earth's interior. Science, 236: 37–48.

Gaherty, J.B. and Lay, T., 1992. Investigation of laterally heterogeneous shear velocity structure in D″ beneath Eurasia. J. Geophys. Res., 97: 417–435.

Garnero, E.J. and Helmberger, D.V., 1993. Travel times of S and SKS: implications for 3-D lower mantle structure. J. Geophys. Res., 98: 8225–8241.

Garnero, E.J., Helmberger, D.V. and Engen, G., 1988. Lateral variations near the core–mantle boundary. Geophys. Res. Lett., 15: 609–612.

Giardini, D., Li, X.-D. and Woodhouse, J.H., 1987. Three-dimensional structure of the Earth from splitting in free oscillations spectra. Nature, 325: 405–411.

Grand, S.P. and Helmberger, D.V., 1985. Upper mantle shear structure beneath Asia from multibounce S waves. Phys. Earth Planet. Inter., 41: 154–169.

Haddon, R.A.W. and Buchbinder, G.G.R., 1987. *S* wave scattering by 3-D heterogeneities at the base of the mantle. Geophys. Res. Lett., 14: 891–894.

Hager, B.H., Clayton, R.W., Richards, M.A., Comer R.P. and Dziewonski, A.M., 1985. Lower mantle heterogeneity, dynamic topography and the geoid. Nature, 313: 541–545.

Helmberger, D.V., 1983. Theory and application of synthetic seismograms. In: H. Kanamori and E. Boschi (Editors) Earthquakes: Observation, Theory and Interpretation. Soc. Italiana di Fisica, Bologna, pp. 173–222.

Knittle, E. and Jeanloz, R., 1991. Earth's core–mantle boundary: results of experiments at high pressures and temperatures. Science, 251: 1438–1443.

Lay, T. and Helmberger, D.V., 1983. A lower mantle S-wave triplication and the shear velocity structure of D″. Geophys. J. R. Astron. Soc., 75: 799–838.

Lay, T. and Young, C.J., 1991. Analysis of seismic SV waves in the core's penumbra. Geophys. Res. Lett., 18: 1373–1376.

Li, X., Giardini D. and Woodhouse, J.H., 1991. Large-scale three-dimensional even-degree structure of the Earth from splitting of long-period normal modes. J. Geophys. Res., 96: 551–577.

Olsen, P. and Kincaid, C., 1991. Experiments on the interaction of thermal convection and compositional layering at the base of the mantle. J. Geophys. Res., 96: 4347–4354.

Revenaugh, J. and Jordan, T.H., 1991. Mantle layering from ScS reverberations 4. The lower mantle and the core–mantle boundary. J. Geophys. Res., 96: 19811–19824.

Sleep, N.H., 1988. Gradual entrainment of a chemical layer at the base of the mantle by overlying convection. Geophys. J. R. Astron. Soc., 95: 437–447.

Su, W., Woodward, R.L. and Dziewonski, A.M., 1992. Joint inversions of travel-time and waveform data for the 3-D models of the Earth up to degree 12. EOS (Trans. Am. Geophys. Union), 73: 201–202 (abstract).

Tanimoto, T., 1990. Long-wavelength S-wave velocity structure throughout the mantle. Geophys. J. Int., 100: 327–336.

Weber, M. and Davis, J.P., 1990. Evidence of a laterally inhomogeneous lower mantle structure from *P*- and *S*-waves. Geophys. J. Int., 102: 231–255.

Woodward, R.L. and Masters, G., 1991. Lower-mantle structure from ScS–S differential travel times. Nature, 352: 231–233.

Young, C.J. and Lay, T., 1987. Evidence for a shear velocity discontinuity in the lowermost mantle beneath India and the Indian Ocean. Phys. Earth Planet. Inter., 49: 37–53.

Young, C.J. and Lay, T., 1990. Multiple phase analysis of the shear velocity structure in the D″ region beneath Alaska. J. Geophys. Res., 95: 17385–17402.